Neurons expressing pathological Tau protein trigger dramatic noninflammatory changes in microglial morphology and dynamics

Rahma Hassan-Abdi[1,2], Alexandre Brenet[1,2], Mohamed Bennis[3], Constantin Yanicostas[1,2] and Nadia Soussi-Yanicostas[1,2*]

[1]INSERM, UMR1141, Hôpital Robert Debré, Paris, France

[2]Université Paris Diderot, Sorbonne Paris Cité, Paris, France

[3]Université Cadi Ayyad, Marrakesh, Morocco

*** Correspondence:**
Dr. Nadia Soussi-Yanicostas
nadia.soussi@inserm.fr

Running title: Imaging microglia and hTau^{P301L}-expressing neurons.

Keywords: Microglia, Tauopathy, Tau protein, Zebrafish, *In vivo* imaging, Tau hyperphosphorylation, Pro-inflammatory cytokines.

Abstract

Microglial cells, the resident macrophages of the brain, are important players in the pathological process of numerous neurodegenerative disorders, including tauopathies, a heterogeneous class of diseases characterized by intraneuronal Tau aggregates. However, microglia response in Tau pathologies remains poorly understood. Here we exploit a genetic zebrafish model of tauopathy, combined with live microglia imaging, to investigate the behavior of microglia *in vivo* in the disease context. Results show that while microglia were almost immobile and displayed long and highly dynamic branches in a wild-type context, in presence of diseased neurons, cells displayed morphological changes, with highly mobile cell bodies together with fewer and shorter processes. We demonstrated that these changes in microglial cells are noninflammatory. We also imaged, for the first time to our knowledge, the phagocytosis of apoptotic tauopathic neurons by microglia *in vivo* and observed that microglia engulfed about as twice materials as in controls. Finally, genetic ablation of microglia in zebrafish tauopathy model significantly increased Tau hyperphosphorylation, suggesting that microglia provide neuroprotection to diseased neurons. Our findings demonstrate for the first time the dynamics of microglia in contact with tauopathic neurons *in vivo* and open perspectives for the real-time study of microglia in many neuronal diseases.

48 ## Introduction

49 Microglia, the resident brain macrophages, are highly plastic and multifunctional cells that
50 continuously monitor the health of neuronal networks (Kierdorf and Prinz, 2017). In a
51 physiological context, microglia display long cytoplasmic processes that constantly extend and
52 retract to contact neighbour neurons and check their physiology (Nimmerjahn et al., 2005; Peri
53 and Nüsslein-Volhard, 2008). Microglia also respond promptly to brain injury or infection, with
54 both immuno-protective and cytotoxic responses, including the secretion of a large set of
55 cytokines (Butovsky and Weiner, 2018; Hanisch, 2002; Hu et al., 2015; Wake et al., 2013) and
56 increased phagocytic capacities to eliminate pathogen debris and dead cells (Leong and Ling,
57 1992; Ling and Wong, 1993; Brockhaus et al., 1996; Nakajima and Kohsaka, 2001; Hanisch and
58 Kettenmann, 2007; Thameem Dheen et al., 2007). However, in some disease contexts, such as
59 tauopathies, microglia also appear to have harmful activities (Bhaskar et al., 2010; Eyo and
60 Dailey, 2013; Maphis et al., 2015; Laurent et al., 2018).

61 Tauopathies are a family of neurodegenerative disorders characterized by intra-neuronal
62 fibrillary aggregates containing abnormally hyperphosphorylated isoforms of the microtubule-
63 associated protein Tau (Alavi Naini and Soussi-Yanicostas, 2015; Spillantini and Goedert, 2013;
64 Wang and Mandelkow, 2016). While the causal role of Tau in the disease is supported by several
65 inherited tauopathies triggered by dominant missense mutations in the protein, such as Tau^{P301L},
66 causing fronto-temporal dementia with parkinsonism on chromosome 17 (FTDP-17) (Hutton et
67 al., 1998), the aetiology of these disorders and the contribution of microglia to their
68 physiopathology remain poorly understood (Hansen et al., 2018; Laurent et al., 2018; Perea et
69 al., 2018).

70 Because of their plasticity and well-established neuroprotective activities, microglial cells
71 are very promising therapeutic targets for the treatment of neuron disorders, including
72 neurodegenerative diseases. However, the scattered distribution of microglia in the brain has so

73 far limited their study to *ex vivo* and *in vitro* approaches that do not faithfully reproduce the
74 complex changing environments of *in vivo* situations. For instance, the classification of mouse
75 microglia cells defined following *ex vivo* approaches, is not readily applicable *in vivo* (Lee et al.,
76 2013; Murray et al., 2014).

77 In an attempt to describe the behavior of microglial cells in a tauopathy disease context *in*
78 *vivo*, we used the transgenic zebrafish Tg(HuC-hTau^{P301L}:DsRed) tauopathy model (Paquet al.,
79 2009) and live microglia imaging (Peri and Nüsslein-Volhard, 2008). We observed that next to
80 hTau^{P301L}-expressing neurons, microglia display dramatic changes in morphology and dynamics,
81 with cells showing fewer and shorter branches and amoeboid-like cell bodies alongside a
82 markedly increased mobility and phagocytic activity. We also imaged the phagocytosis of dying
83 neurons by microglia and showed that these cells could phagocyte nearly twice as much as in
84 homeostatic brains. However, we also observed that these microglial cells failed to phagocyte
85 all dead neurons, highlighting the limits of their phagocyting abilities.

86 Results

87 Microglia display dramatic changes in shape and dynamics in the presence of hTau^{P301L}-
88 expressing neurons

89 To investigate the behavior of microglial cells in a tauopathy disease context *in vivo*, we
90 used the transgenic Tg(HuC-hTau^{P301L}:DsRed) zebrafish model of Tau-induced
91 neurodegeneration, combined with the transgenic Tg(ApoE-eGFP) microglia marker line. As
92 previously shown, in the optic tectum of Tg(ApoE-eGFP) embryos, microglia displayed a
93 ramified morphology, with a small cell body and several elongated branches (Figures 1A,C). By
94 contrast, in Tg(ApoE-eGFP; HuC-hTau^{P301L}:DsRed) embryo microglia displayed a rounder
95 morphology, with a larger cell body and fewer, shorter branches (Figures 1B,B',D).
96 Quantifications of morphological parameters confirmed these dramatic changes in microglia
97 morphology seen in the presence of diseased neurons, with a smaller surface area (Figure 1E)

98 and volume (Figure 1F); and a greater sphericity (Figure 1G). However, alongside these rounded
99 microglia, a few branched cells were also observed in the disease context (Figures 1B, B').

100 Given that microglial cells are highly dynamic, we used *in vivo* real-time confocal imaging
101 combined with Imaris software (Bitplane Inc.) image analysis to determine whether the presence
102 of hTau^{P301L}-expressing neurons modified microglia dynamics. In Tg(ApoE-eGFP) embryos,
103 microglia displayed dynamic processes that were constantly extending and retracting, while
104 their cell bodies remained almost immobile (Figures 1H,J, Video 1, Supplementary figures 1A,C,
105 Video 5). By contrast, in Tg(ApoE-eGFP; HuC-hTau^{P301L}:DsRed) embryos, microglia were
106 highly mobile with their cell bodies traveling over longer distances (Figures 1I,K, Video 2,
107 Supplementary figures 1B,D, Video 6). Quantifications of microglia dynamics confirmed that in
108 the presence of hTau^{P301L}-expressing neurons, microglia displayed increased mean speed (Figure
109 1L) and mean track displacement of the processes (Figure 1M), and a much larger displacement
110 of the cell bodies over a similar time frame (Figure 1N).

111 To further characterize the phenotype of these microglial cells, we analysed the expression
112 levels of two pro-inflammatory cytokines, IL-1β and IL-8, in the brain tissue of the transgenic
113 Tg(HuC-hTau^{P301L}:DsRed) and wild-type embryos (Figures 1O,P). Interestingly, neither of these
114 cytokines were overexpressed in the pathologic context, the two tested groups displaying no
115 significant differences in expression levels of either IL-1β or IL-8, indicating that microglial cells
116 in the transgenic Tg(HuC-hTau^{P301L}:DsRed) were not in pro-inflammatory states.

117

118 **Genetic depletion of microglia worsens pathology in Tg(HuC-hTau^{P301L}:DsRed) embryos**

119 As a first attempt to investigate the function of microglial cells in Tau pathology, we
120 generated Tg(HuC-hTau^{P301L}:DsRed) embryos completely devoid of microglia following injection
121 of an antisense morpholino oligonucleotide targeting pU.1 (MO-pU1) transcripts encoding a

122 transcription factor essential for proper differentiation of macrophage/microglia (Rhodes et al.,
123 2005), and then studied the consequences of such microglial cell ablation on Tau
124 phosphorylation, neuron apoptosis and expression of pro-inflammatory cytokines. Injection of
125 the MO-pU1 (Figure 2A) leads to a complete absence of microglial cells in the brain of the
126 embryos as shown by either Neutral Red staining (Figure 2B), or immunocytochemistry using
127 L-plastin antibody (Figure 2C).

128 Using 5 dpf wild-type and transgenic Tg(HuC-hTau^{P301L}:DsRed) embryos with or without
129 microglial cells, we then studied the consequences of microglia ablation on the expression of pro-
130 inflammatory cytokines IL-1β and IL-8. Results showed that while expression of Tau^{P301L} did
131 not stimulate overexpression of IL-1β (Figure 2D) and IL-8 (Figure 2E) in microglia-containing
132 embryos, microglia depletion in Tg(HuC-hTau^{P301L}:DsRed) embryos provoked a markedly
133 increased expression of both pro-inflammatory cytokines, suggesting that microglia mitigate
134 pro-inflammatory activities elicited by other glial cells, likely astrocytes.

135 As a first attempt to determine the effect of microglia absence on Tau hyperphosphorylation
136 *in vivo*, we quantified phosphorylation levels at Ser396 site on hTau protein in Tg(HuC-
137 hTau^{P301L}:DsRed) embryos with and without microglia (Figure 2F). Genetic ablation of microglia
138 in Tg(HuC-hTau^{P301L}:DsRed) embryos increased the accumulation of hyperphosphorylated Tau
139 when compared to their siblings with microglia (Figure 2F, with microglia *vs.* without
140 microglia). Quantification of pTau/total Tau ratio confirmed that hTau protein
141 phosphorylation level was significantly increased in microglia-depleted Tg(HuC-
142 hTau^{P301L}:DsRed) embryos (Figure 2G). To further investigate the effects of microglial ablation
143 on Tau hyperphosphorylation, Tg(HuC-hTau^{P301L}:DsRed) embryos devoid of microglia were
144 analysed by immunohistochemistry using the antibody PHF1, targeting two phosphorylation
145 sites, Ser396 site and pathological phosphorylation site Ser404, on hTau protein (PHF1)
146 (Figures 2H,I). In good agreement with Western blot analysis, a significant increase in PHF1
147 labelling intensity was observed in the telencephalon of 6 dpf Tg(HuC-hTau^{P301L}:DsRed; *nlrc3-*

148 *like*$^{st73/73}$) mutant embryos devoid of microglia (Figure 2I) when compared to that observed in
149 the brain of their siblings with microglia (Figure 2H). The quantification of the ratio of
150 hyperphosphorylated human Tau protein on brain sections from Tg(HuC-hTau^{P301L}:DsRed;
151 *nlrc3-like*$^{st73/73}$) embryos confirmed the significant increase of this ratio displayed in protein
152 extracts from Tg(HuC-hTau^{P301L}:DsRed) embryos microglia-depleted with morpholino (Figure
153 2J).

154

155 **Microglia phagocytic activity is enhanced in the presence of hTau^{P301L}-expressing neurons**

156 As phagocytosis is a main feature of microglial cells, we first monitored the phagocytic
157 activity of microglia in Tg(ApoE-eGFP; HuC-hTau^{P301L}:DsRed) embryos. We observed the
158 phagocytosis of hTau^{P301L}-expressing neurons by microglia, using confocal real-time imaging
159 (Figure 3B, Video 3). A microglial cell in the optic tectum (Figures 3B,C,0 min) sends one of
160 its processes to the pathological neuron (Figures 3B,C,5 min) to draw it towards its cell body
161 (Figures 3B,C,9 min) and execute the digestion of the neuron and its debris until completion of
162 the process (Figures 3B,C,18 min). We also observed the detail of a microglial cell engulfing
163 three neurons simultaneously (Supplementary figure 2, Video 7).We next assessed the
164 phagocytic activity of microglia by quantifying the total engulfed volume, which appeared
165 higher in Tg(ApoE-eGFP; HuC-hTau^{P301L}:DsRed) embryos (Figure 3D). Given the critical role
166 of microglia in removing apoptotic cells and other noxious bodies, we next visualized neuronal
167 death in Tg(ApoE-eGFP; HuC-hTau^{P301L}:DsRed) embryos using the apoptotic marker Acridine
168 Orange. Data showed that microglia specifically engulfed apoptotic neurons (Figures 3E-H,
169 Video 4) but not non-apoptotic hTau^{P301L}-expressing cells, supporting the notion that microglia
170 specifically responds to signals sent by degenerating neurons that are already apoptotic but not
171 hTau^{P301L}-expressing neurons *per se*. However, quantification of the number of non-engulfed
172 apoptotic neurons in Tg(ApoE-eGFP; HuC-hTau^{P301L}:DsRed) and control Tg(ApoE-eGFP;

173 HuC-RFP) embryos showed that microglia failed to phagocyte all apoptotic hTau^{P301L}-expressing
174 neurons compared with control neurons (Figure 3I).

175 Discussion

176 To date, almost all studies aimed at investigating the physiology of microglia or their
177 interactions with neurons in rodent models of neuronal diseases have relied widely on *ex vivo*
178 and *in vitro* approaches, which cannot accurately reproduce the complexity of the physiological
179 conditions observed in living brains (Bemiller et al., 2017; Hickman et al., 2013; Maphis et al.,
180 2015; Rustenhoven et al., 2018).

181 While these marker-based approaches remain useful to gather prerequisite knowledge on
182 immune cells, it is nonetheless crucial to preserve the morphology and dynamics of these highly
183 plastic cells, which respond to very small changes in the CNS, and so to study them in a living
184 brain (He et al., 2018). Recent studies show that time spent by microglia *ex vivo* is associated
185 with a different evolution of gene expression until their expression levels become the reverse of
186 the initial measures (Gosselin et al., 2017).

187 The present work is, to our knowledge, the first aimed at characterizing the dynamic behavior
188 of microglial cells in the presence of pathological neurons expressing a mutant human Tau
189 protein, hTau^{P301L}, causing tauopathy.

190 Our results show that the presence of these hTau^{P301L}-expressing neurons caused dramatic
191 changes to microglia, with the cells displaying an amoeboid-like shape and higher mobility.
192 Although these morphological and dynamic changes are reminiscent of the classical microglial
193 activation profile in response to injury or disease (Nakajima and Kohsaka, 2001), these rounded
194 microglial cells did not overexpress assessed pro-inflammatory cytokines, IL-1β and IL-8,
195 showing that the observed changes were noninflammatory (Zhao et al., 2018). On the contrary,
196 the genetic depletion of microglia in these pathological brains was paired with a more than 2-

197 fold increase in the expression levels of these pro-inflammatory cytokines. This outcome, similar
198 to that of a study of prion-induced neurodegeneration in mice (Zhu et al., 2016), may be linked
199 to astrocytes, the largest glial group, which can also produce pro-inflammatory factors and
200 exhibit a reactive state in tauopathy mice models (Sidoryk-Wegrzynowicz et al., 2017), likely
201 exacerbated by the higher levels of pathological hyperphosphorylated Tau protein, which can
202 be taken up by astrocytes (Martini-Stoica et al., 2018; Perea et al., 2019).

203 These noninflammatory, highly dynamic microglial cells displayed an intense phagocytic
204 activity, specifically eliminating nearly twice as many apoptotic neurons as microglial cells in
205 healthy brains. However, a significantly higher number of unengulfed apoptotic neurons in
206 tauopathic brains suggests that these microglial cells are overwhelmed by an excessive neuronal
207 death rate generated in this transgenic model. One therapeutic approach might thus be to
208 enhance the phagocytic activity of microglia to slow disease spread.

209 This complete study in an intact brain visualizes interactions between microglia and
210 hTau^{P301L}-expressing neurons in real time and sheds light on noninflammatory microglia that
211 exerts a protective role mainly through specific phagocytosis of apoptotic hTau^{P301L}-expressing
212 neurons, thereby limiting the spread of noxious overspills or pathologic hyperphosphorylated
213 Tau. However, while displaying enhanced phagocytic activity towards hTau^{P301L}-expressing
214 neurons and efficiently eliminating dead neurons, microglial cells appeared overwhelmed, as
215 evidenced by the higher number of unengulfed dead neurons in the transgenic embryo brains.
216 These findings support therapeutic approaches based on the modulation of microglial phagocytic
217 activity in a specific neurodegenerative context.

218

219

220

221 ## Materials and methods

222 ### Ethics statement

223 All the animal experiments described in the present study were conducted at the French
224 National Institute of Health and Medical Research (INSERM) UMR 1141 in Paris in accordance
225 with European Union guidelines for the handling of laboratory animals
226 (http://ec.europa.eu/environment/chemicals/lab_animals/home_en.htm) and were approved
227 by the Direction Départementale de la Protection des Populations de Paris and the French
228 Animal Ethics Committee under reference No. 2012-15/676-0069.

229 ### Zebrafish lines and maintenance

230 Zebrafish were maintained at 26.5 °C in 14 h light and 10 h dark cycles. Embryos were collected
231 by natural spawning and to avoid pigmentation, 0.003% 1-phenyl-2-thiourea (PTU) was added
232 at 1 dpf (day post-fertilization). The transgenic lines Tg(HuC-hTau^{P301L}:DsRed) (Paquet et al.,
233 2009) and Tg(ApoE-eGFP)(Peri and Nüsslein-Volhard, 2008) and *nlrc3-like*$^{st73/st73}$ mutants
234 (Shiau et al., 2013) have been previously described.

235 ### Confocal imaging

236 For *in vivo* imaging, 7 dpf larvae were anaesthetized with 112 µg/ml 3-aminobenzoic acid ethyl
237 ester (tricaine, Sigma), immobilized in 1.2% low melting-point agarose in the centre of a 35 mm
238 glass-bottomed dish (Corning®), and covered with E3 medium containing 112 µg/ml tricaine.
239 Images were acquired using a Leica SP8 confocal scanning laser microscope equipped with a
240 Leica 20x/0.75 multi-immersion objective and an Olympus 40x/1.1 water objective; and a Leica
241 DM6000FS Spinning disk L2 microscope equipped with a Leica 25x/0.95 water immersion
242 objective. All the images were then processed using LAS-X (Leica), MetaMorph 7.8.9 (Molecular
243 Devices), AutoQuant X3.1.1 (Media Cybernetics), Fiji (Version 2.0.0-rc-65/1.52b) and Adobe
244 Photoshop 7.0 (Adobe System).

245 **Image analysis**

246 The surface area, volume and sphericity ($\Psi = \frac{\pi^{\frac{1}{3}}(6V_p)^{\frac{2}{3}}}{A_p}$) of microglial cells were quantified using
247 Imaris MeasurementPro (Bitplane Inc.). The speed (distance travelled per unit time) and
248 displacement (distance between first and last positions) of microglial processes were analysed
249 using Imaris Filament tracer (Bitplane Inc.) on 15 minutes long time-lapses. Microglial cell body
250 displacement (distance between first and last positions) was tracked with Imaris
251 MeasurementPro on 30 minutes long time-lapses. Three-dimensional cell reconstructions were
252 created using Imaris MeasurementPro.

253 **Ablation of microglia**

254 Morpholino pU.1 (MO-pU1): 5'-GATATACTGATACTCCATTGGTGGT-3' was obtained
255 from Gene Tools. 2 nl of a 0.5 mM solution, corresponding to 1 pmol of pU.1 morpholino was
256 injected into 1 to 2 cells stage embryos using standard protocols. After injection, the embryos
257 were incubated in E3 medium at 28.5 °C until analysis at the desired stage. To select embryos
258 in which microglia differentiation was efficiently blocked, Neutral Red staining was used to label
259 microglia. Embryos were incubated in Neutral Red diluted in E3 medium for 5-8 hours at
260 28.5 °C, and rinsed 10 min before examination using a stereomicroscope (Zeiss).

261 **Apoptosis labelling**

262 To observe apoptotic neurons, embryos were incubated in Acridine Orange solution (1:500,
263 VectaCell) for 20 min at 28.5 °C in the dark, and rinsed twice for 10 min in E3 medium.
264 Although both GFP from microglia and acridine orange have very close excitation and emission
265 spectra, their signal is distinguishable, as acridine orange labelled neuronal cell bodies emit a
266 greater fluorescence. Therefore, GFP channel (green) also shows Acridine Orange staining (blue)
267 (Figure 3F).

268 **Immunocytochemistry**

269 6 dpf Tg(HuC-hTau^{P301L}:DsRed) and Tg(HuC-hTau^{P301L}:DsRed; *nlrc3-like*$^{st73/73}$) embryos were
270 anaesthetized in 0.2% tricaine, fixed with 4% paraformaldehyde, cryoprotected in 10% sucrose
271 solution prior to flash freezing in isopentane. Samples were stored at -80°C until use. Embryos
272 were cut into 20 µm thick sections on cryostat, mounted on superfrost slides, and stored at -
273 80°C. Cryosections (20 µm) were fixed in 4% paraformaldehyde at room temperature for 10
274 min. After washing thrice with PBS, sections were treated with 0.25% trypsin in 1X PBS for 2
275 min at 25°C. Immunohistochemistry was performed as previously described (Puverel et al.,
276 2009). Briefly, sections were blocked and permeabilized with 0.2% gelatin, 0.25% Triton X-100
277 diluted in 1X PBS for 1 hr at room temperature and then incubated overnight at room
278 temperature with anti-PHF1 (1:100, mouse monoclonal, gift of Dr. Peter Davies, Albert Einstein
279 College of Medicine, New York, USA) After several washes, sections were incubated for 1 hr
280 with the donkey anti-mouse coupled to Alexa Fluor 488 (1:500, Jackson Laboratories, West
281 Grove, PA). Sections were counterstained for 10 min with 0.1% DAPI (Sigma-Aldrich) before
282 being mounted with Vectashield Mounting Medium (Vector). Sections were analyzed using a
283 Leica TCS SP8 confocal scanning system (Leica Microsystems). Images were acquired using a
284 Leica SP8 confocal scanning laser microscope equipped with a Leica 20x/0.75 multi-immersion
285 objective. Images were processed with LAS-X (Leica), Fiji (Version 2.0.0-rc-65/1.52b) and
286 Adobe Photoshop 7.0 (Adobe System).

287 For whole mount immunostaining, 5 dpf wild-type embryos with or without microglia, were
288 fixed in 4% formaldehyde in PBS for 1 hour 30 minutes at room temperature, washed three
289 times in PBS (10 minutes each) and permeabilized in cold acetone (-20°C) for 20 minutes. After
290 several washes, embryos were incubated in collagenase solution for 1 hour.
291 Immunocytochemistry was performed as described previously (Naini et al., 2018) using rabbit
292 anti-zebrafish L-plastin polyclonal antibody (gift of Dr. Michael Redd, University College
293 London, United Kingdom), followed by Alexa-coupled secondary anti-rabbit antibody
294 (Molecular Probes) at 1:500 dilution. After washing, the fluorescence was analyzed using a Leica

295 TCS SP8 confocal scanning system (Leica Microsystems). Images were collected using a Leica
296 20x/0.75 multi-immersion objective. Images were processed with LAS-X (Leica), Fiji (Version
297 2.0.0-rc-65/1.52b) and Adobe Photoshop 7.0 (Adobe System).

298 **RT-qPCR**

299 Total RNAs were extracted from independent batches of 15 embryos each, using the NucleoSpin
300 RNA kit (Macherey Nagel, Germany). The integrity and concentration of RNAs were assessed
301 by spectrophotometry using a Nanodrop™ device (Thermoscientific, USA). Total RNA (1µg)
302 samples were reverse transcribed using the iScript™ cDNA synthesis kit (Bio-Rad, USA). RT-
303 qPCR experiments were performed in triplicate using SYBR Green Super-mix (Bio-Rad, USA)
304 according to a program of 40 cycles in 3 steps (denaturation of 5 seconds at 96 ° C, hybridization
305 of 10 seconds at 60 ° C and extension of 10 seconds at 72 ° C). Primers were designed manually
306 following visual inspection of gene sequences. Gene sequences and NCBI references are given in
307 **Supplementary table 1**. Specific mRNA levels were evaluated after normalization of the results
308 with tubulin-α (tuba1) mRNA as reference, and the results were indicated in arbitrary units
309 determined respectively to the levels of RNA determined in wild-type embryos.

310 **Western blot**

311 Embryos at 5 dpf were collected, anaesthetized and lysed on ice with lysis buffer (50 mM Tris-
312 HCl, 320mM Sucrose, pH 7.4) supplemented with protease and phosphatase inhibitors (Roche).
313 Lysates were homogenized by sonication (thrice 10 seconds) and centrifuged at 600 g for 10
314 min. Samples containing 10 µg proteins were subjected to SDS-PAGE in 4-20% gradient
315 acrylamide gel. Primary antibody against phosphorylated tau, Ser396 (1:1000, mouse
316 monoclonal, Ozyme); and anti-human total tau antibody (1:1000, rabbit polyclonal, Dako
317 Cytomation) were used. Subsequently, the blots were incubated for 1 hour at room temperature
318 with the corresponding secondary antibodies (anti-mouse or anti-rabbit, 1:5000, Cell Signalling

319 Technology) diluted in bovine serum albumin solution and developed with ECL RevelBlOt®
320 Plus (Ozyme) following manufacturer's instructions.

321 **Statistics**

322 All statistics were assessed using a Welch two-sample *t*-test or an ANOVA followed by a Tukey
323 post-test. All data are represented as means ± SEM.

324 **Conflict of Interest**

325 The authors declare that the research was conducted in the absence of any commercial or
326 financial relationships that could be construed as a potential conflict of interest.

327 **Funding**

328 This work was supported by Institut National de la Santé et la Recherche Médicale
329 (INSERM), the National Center for Scientific Research (CNRS), the French National
330 Research Agency (ANR-16-CE18-0010), and Fondation NRJ (Institut de France) to NSY.
331 Funding sources had no involvement in study design, collection, analysis or interpretation of
332 data, or decision to publish.

333 **Acknowledgments**

334 We thank Bettina Schmid (DZNE, Munich, Germany) for providing us with the Tg(HuC-
335 hTau^{P301L}:DsRed) transgenic line, Francesca Peri (University of Zurich, Zurich, Switzerland) for
336 providing us with the Tg(ApoE-eGFP) and Michael Redd (University College London, London,
337 United Kingdom) for providing us with the rabbit anti-zebrafish L-plastin polyclonal antibody.
338 We also thank the imaging facility IMAG'IC (Cochin Institute, Paris). We also thank Christiane
339 Romain and Olivier Bar (INSERM UMR 1141) for their technical assistance.

340

Bibliography

Alavi Naini, S. M., and Soussi-Yanicostas, N. (2015). Tau Hyperphosphorylation and Oxidative Stress, a Critical Vicious Circle in Neurodegenerative Tauopathies? *Oxid. Med. Cell. Longev.* 2015. doi:10.1155/2015/151979.

Bemiller, S. M., McCray, T. J., Allan, K., Formica, S. V., Xu, G., Wilson, G., et al. (2017). TREM2 deficiency exacerbates tau pathology through dysregulated kinase signaling in a mouse model of tauopathy. *Mol. Neurodegener.* 12. doi:10.1186/s13024-017-0216-6.

Bhaskar, K., Konerth, M., Kokiko-Cochran, O. N., Cardona, A., Ransohoff, R. M., and Lamb, B. T. (2010). Regulation of Tau Pathology by the Microglial Fractalkine Receptor. *Neuron* 68, 19. doi:10.1016/j.neuron.2010.08.023.

Brockhaus, J., Möller, T., and Kettenmann, H. (1996). Phagocytozing ameboid microglial cells studied in a mouse corpus callosum slice preparation. *Glia* 16, 81–90. doi:10.1002/(SICI)1098-1136(199601)16:1<81::AID-GLIA9>3.0.CO;2-E.

Butovsky, O., and Weiner, H. L. (2018). Microglial signatures and their role in health and disease. *Nat. Rev. Neurosci.* doi:10.1038/s41583-018-0057-5.

Eyo, U. B., and Dailey, M. E. (2013). Microglia: Key elements in neural development, plasticity, and pathology. *J. Neuroimmune Pharmacol.* 8, 494–509. doi:10.1007/s11481-013-9434-z.

Gosselin, D., Gosselin, D., Skola, D., Coufal, N. G., Holtman, I. R., Johannes, C. M., et al. (2017). An environment-dependent transcriptional network specifies human microglia identity. 3222, 33–35.

Hanisch, U. K. (2002). Microglia as a source and target of cytokines. *Glia* 40, 140–155. doi:10.1002/glia.10161.

Hanisch, U. K., and Kettenmann, H. (2007). Microglia: Active sensor and versatile effector cells in the normal and pathologic brain. *Nat. Neurosci.* 10, 1387–1394. doi:10.1038/nn1997.

Hansen, D. V., Hanson, J. E., and Sheng, M. (2018). Microglia in Alzheimer's disease. *J. Cell Biol.* 217, 459–472. doi:10.1083/jcb.201709069.

He, Y., Yao, X., Taylor, N., Bai, Y., Lovenberg, T., and Bhattacharya, A. (2018). RNA sequencing analysis reveals quiescent microglia isolation methods from postnatal mouse brains and limitations of BV2 cells. *J. Neuroinflammation* 15. doi:10.1186/s12974-018-1195-4.

373 Hickman, S. E., Kingery, N. D., Ohsumi, T. K., Borowsky, M. L., Wang, L., Means, T. K., et
374 al. (2013). The microglial sensome revealed by direct RNA sequencing. *Nat. Neurosci.* 16,
375 1896–1905. doi:10.1038/nn.3554.

376 Hu, X., Leak, R. K., Shi, Y., Suenaga, J., Gao, Y., Zheng, P., et al. (2015). Microglial and
377 macrophage polarization - New prospects for brain repair. *Nat. Rev. Neurol.* 11, 56–64.
378 doi:10.1038/nrneurol.2014.207.

379 Hutton, M., Lendon, C. L., Rizzu, P., Baker, M., Froelich, S., Houlden, H. H., et al. (1998).
380 Association of missense and 5'-splice-site mutations in tau with the inherited dementia
381 FTDP-17. *Nature* 393, 702–704. doi:10.1038/31508.

382 Kierdorf, K., and Prinz, M. (2017). Microglia in steady state. *J. Clin. Invest.* 127, 3201–3209.
383 doi:10.1172/JCI90602.

384 Laurent, C., Buée, L., and Blum, D. (2018). Tau and neuroinflammation: What impact for
385 Alzheimer's Disease and Tauopathies? *Biomed. J.* 41, 21–33. doi:10.1016/j.bj.2018.01.003.

386 Lee, D. C., Rizer, J., Hunt, J. B., Selenica, M.-L. B., Gordon, M. N., and Morgan, D. (2013).
387 Experimental manipulations of microglia in mouse models of Alzheimer's pathology.
388 Activation reduces amyloid but hastens tau pathology. *Neuropathol. Appl. Neurobiol.* 39,
389 69. doi:10.1111/nan.12002.

390 Leong, S. -K, and Ling, E. -A (1992). Amoeboid and ramified microglia: Their
391 interrelationship and response to brain injury. *Glia* 6, 39–47. doi:10.1002/glia.440060106.

392 Ling, E. -A, and Wong, W. -C (1993). The origin and nature of ramified and amoeboid
393 microglia: A historical review and current concepts. *Glia* 7, 9–18.
394 doi:10.1002/glia.440070105.

395 Maphis, N., Xu, G., Kokiko-cochran, O. N., Cardona, A., Ransohoff, R. M., Lamb, B. T., et
396 al. (2015a). Loss of tau rescues inflammation-mediated neurodegeneration. *Front.*
397 *Neurosci.* 9, 1–12. doi:10.3389/fnins.2015.00196.

398 Maphis, N., Xu, G., Kokiko-Cochran, O. N., Jiang, S., Cardona, A., Ransohoff, R. M., et al.
399 (2015b). Reactive microglia drive tau pathology and contribute to the spreading of
400 pathological tau in the brain. *Brain* 138, 1738–1755. doi:10.1093/brain/awv081.

401 Martini-Stoica, H., Cole, A. L., Swartzlander, D. B., Chen, F., Wan, Y.-W., Bajaj, L., et al.
402 (2018). TFEB enhances astroglial uptake of extracellular tau species and reduces tau
403 spreading. *J. Exp. Med.* 215, 2355–2377. doi:10.1084/JEM.20172158.

404 Murray, P. J., Allen, J. E., Biswas, S. K., Fisher, E. A., Gilroy, D. W., Goerdt, S., et al.

(2014). Macrophage Activation and Polarization: Nomenclature and Experimental Guidelines. *Immunity* 41, 14–20. doi:10.1016/j.immuni.2014.06.008.

Naini, S. M. A., Yanicostas, C., Hassan-Abdi, R., Blondeel, S., Bennis, M., Weiss, R. J., et al. (2018). Surfen and oxalyl surfen decrease tau hyperphosphorylation and mitigate neuron deficits in vivo in a zebrafish model of tauopathy. *Transl. Neurodegener.* 7, 6. doi:10.1186/s40035-018-0111-2.

Nakajima, K., and Kohsaka, S. (2001a). Microglia: Activation and their significance in the central nervous system. *J. Biochem.* doi:10.1093/oxfordjournals.jbchem.a002969.

Nakajima, K., and Kohsaka, S. (2001b). Microglia: Activation and their significance in the central nervous system. Oxford University Press doi:10.1093/oxfordjournals.jbchem.a002969.

Nimmerjahn, A., Kirchhoff, F., and Helmchen, F. (2005). Resting microglial cells are highly dynamic surveillants of brain parenchyma in vivo. *Science (80-.).* 308, 1314–1318. doi:10.1126/science.1110647.

Paquet, D., Bhat, R., Sydow, A., Mandelkow, E. M., Berg, S., Hellberg, S., et al. (2009). A zebrafish model of tauopathy allows in vivo imaging of neuronal cell death and drug evaluation. *J. Clin. Invest.* 119, 1382–1395. doi:10.1172/JCI37537.

Perea, J. R., Llorens-Martín, M., Ávila, J., and Bolós, M. (2018). The Role of Microglia in the Spread of Tau: Relevance for Tauopathies. *Front. Cell. Neurosci.* 12. doi:10.3389/fncel.2018.00172.

Perea, J. R., López, E., Díez-Ballesteros, J. C., Ávila, J., Hernández, F., and Bolós, M. Extracellular Monomeric Tau Is Internalized by Astrocytes. *Front. Neurosci.* doi:10.3389/fnins.2019.00442.

Peri, F., and Nüsslein-Volhard, C. (2008). Live Imaging of Neuronal Degradation by Microglia Reveals a Role for v0-ATPase a1 in Phagosomal Fusion In Vivo. *Cell* 133, 916–927. doi:10.1016/j.cell.2008.04.037.

Puverel, S., Nakatani, H., Parras, C., and Soussi-Yanicostas, N. (2009). Prokineticin receptor 2 expression identifies migrating neuroblasts and their subventricular zone transient-amplifying progenitors in adult mice. *J. Comp. Neurol.* 512, 232–242. doi:10.1002/cne.21888.

Rhodes, J., Hagen, A., Hsu, K., Deng, M., Liu, T. X., Look, A. T., et al. (2005). Interplay of pu.1 and Gata1 determines myelo-erythroid progenitor cell fate in zebrafish. *Dev. Cell* 8, 97–108. doi:10.1016/j.devcel.2004.11.014.

438 Rustenhoven, J., Smith, A. M., Smyth, L. C., Jansson, D., Scotter, E. L., Swanson, M. E. V.,
439 et al. (2018). PU.1 regulates Alzheimer's disease-associated genes in primary human
440 microglia. *Mol. Neurodegener.* 13. doi:10.1186/s13024-018-0277-1.

441 Shiau, C. E., Monk, K. R., Joo, W., and Talbot, W. S. (2013). An Anti-inflammatory NOD-
442 like Receptor Is Required for Microglia Development. *Cell Rep.* 5, 1342–1352.
443 doi:10.1016/j.celrep.2013.11.004.

444 Sidoryk-Wegrzynowicz, M., Gerber, Y. N., Ries, M., Sastre, M., Tolkovsky, A. M., and
445 Spillantini, M. G. (2017). Astrocytes in mouse models of tauopathies acquire early deficits
446 and lose neurosupportive functions. *Acta Neuropathol. Commun.* 5, 89.
447 doi:10.1186/s40478-017-0478-9.

448 Sousa, C., Golebiewska, A., Poovathingal, S. K., Kaoma, T., Pires-Afonso, Y., Martina, S., et
449 al. (2018). Single-cell transcriptomics reveals distinct inflammation-induced microglia
450 signatures. *EMBO Rep.* doi:10.15252/embr.201846171.

451 Spillantini, M. G., and Goedert, M. (2013). Tau pathology and neurodegeneration. *Lancet*
452 *Neurol.* 12, 609–622. doi:10.1016/S1474-4422(13)70090-5.

453 Thameem Dheen, S., Kaur, C., and Ling, E.-A. (2007). Microglial Activation and its
454 Implications in the Brain Diseases. *Curr. Med. Chem.* 14, 1189–1197.
455 doi:http://dx.doi.org/10.2174/092986707780597961.

456 Wake, H., Moorhouse, A. J., Miyamoto, A., and Nabekura, J. (2013). Microglia: Actively
457 surveying and shaping neuronal circuit structure and function. *Trends Neurosci.* 36, 209–
458 217. doi:10.1016/j.tins.2012.11.007.

459 Wang, Y., and Mandelkow, E. (2016). Tau in physiology and pathology. *Nat. Rev. Neurosci.*
460 17, 5–21. doi:10.1038/nrn.2015.1.

461 Zhao, X., Liao, Y., Morgan, S., Mathur, R., Feustel, P., Mazurkiewicz, J., et al. (2018).
462 Noninflammatory Changes of Microglia Are Sufficient to Cause Epilepsy. *Cell Rep.* 22,
463 2080–2093. doi:10.1016/j.celrep.2018.02.004.

464 Zhu, C., Herrmann, U. S., Falsig, J., Abakumova, I., Nuvolone, M., Schwarz, P., et al. (2016).
465 A neuroprotective role for microglia in prion diseases. *J. Exp. Med.* 213, 1047–59.
466 doi:10.1084/jem.20151000.

467

468

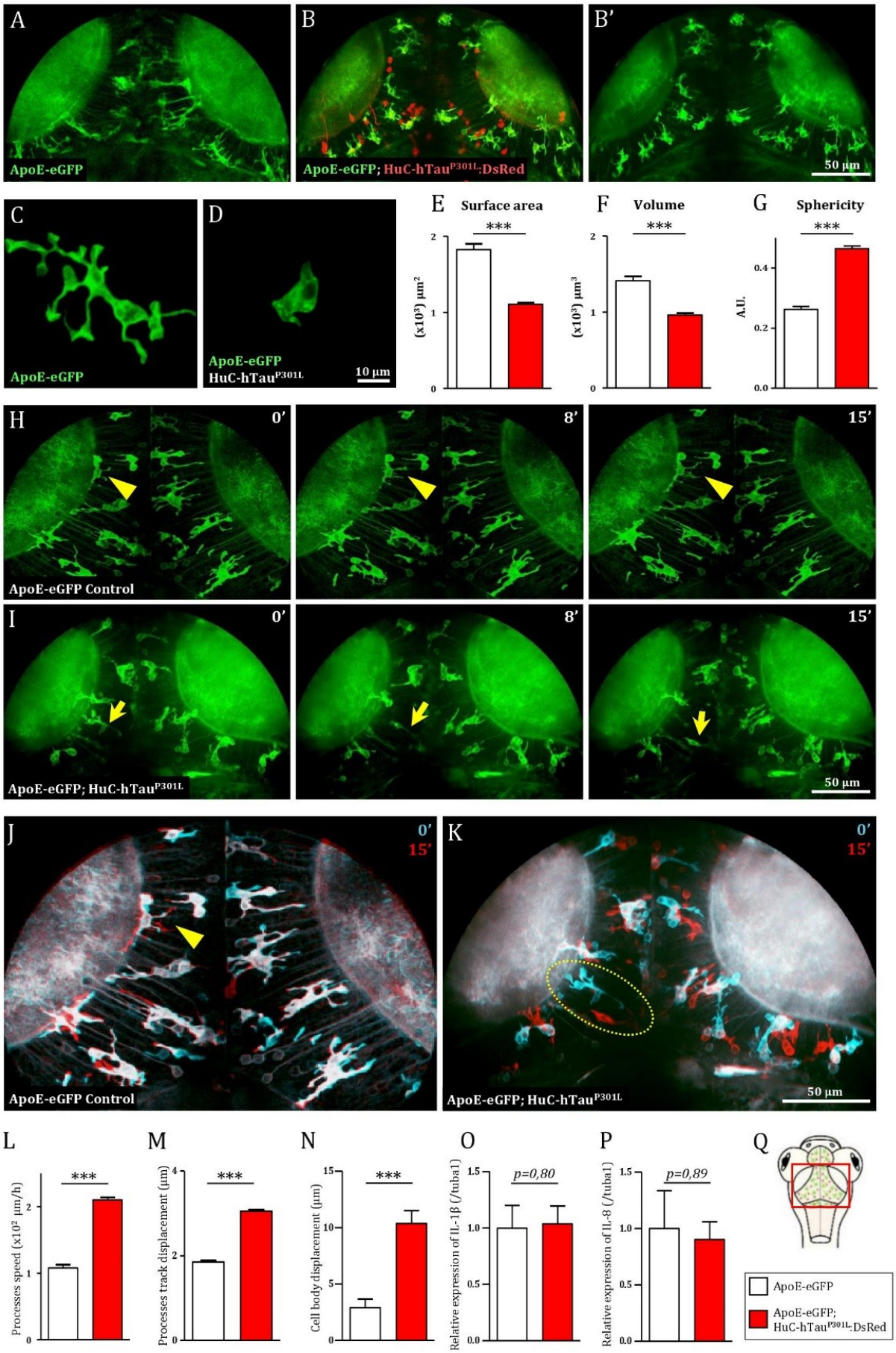
A
ApoE-eGFP
B
ApoE-eGFP; HuC-hTau^{P301L}:DsRed
B'
50 µm
C
ApoE-eGFP
D
ApoE-eGFP
HuC-hTau^{P301L}
10 µm
E Surface area
***
(x10³) µm²
F Volume
***
(x10³) µm³
G Sphericity
***
A.U.
H
0'
8'
15'
ApoE-eGFP Control
I
0'
8'
15'
ApoE-eGFP; HuC-hTau^{P301L}
50 µm
J
0'
15'
ApoE-eGFP Control
K
0'
15'
ApoE-eGFP; HuC-hTau^{P301L}
50 µm
L
***
Processes speed (x10² µm/h)
M
***
Processes track displacement (µm)
N
***
Cell body displacement (µm)
O
p=0,80
Relative expression of IL-1β (/tuba1)
P
p=0,89
Relative expression of IL-8 (/tuba1)
Q
ApoE-eGFP
ApoE-eGFP; HuC-hTau^{P301L}:DsRed

492 **Figure 1. Noninflammatory microglia displays dramatic changes in morphology and**
493 **dynamics in the presence of hTau^{P301L}–expressing neurons.** (**A, B, B'**) Dorsal views of the
494 optic tectum of 7 dpf Tg(ApoE-eGFP) (**A**) and Tg(ApoE-eGFP; HuC-hTau^{P301L}:DsRed)
495 transgenic embryos (**B, B'**), showed the characteristic ramified morphology of microglia in wild-
496 type (**A**), while in the presence of hTau^{P301L}-expressing neurons, microglial cells displayed shorter
497 processes and larger cell bodies. (**C, D**) Detailed morphology of microglial cells in Tg(ApoE-
498 eGFP) (**C**) and Tg(ApoE-eGFP; HuC-hTau^{P301L}:DsRed) embryos (**D**). (**E-G**) Measurements of
499 microglia morphological parameters; surface area (**E**, $p < 0.0001$), volume (**F**, $p < 0.0001$) and
500 sphericity (**G**, $p < 0.0001$), in Tg(ApoE-eGFP) (n=10) and Tg(ApoE-eGFP; HuC-
501 hTau^{P301L}:DsRed) (n=24) embryos, confirmed the cell shape changes observed in the presence
502 of hTau^{P301L}-expressing neurons. (**H, I**) Time-lapse sequences of microglia dynamics in Tg(ApoE-
503 eGFP) (**H**, Video 1) and Tg(ApoE-eGFP; HuC-hTau^{P301L}:DsRed) embryos (**I**, Video 2). (**J, K**)
504 Merged images of two time points separated by 15 minutes from video 1 (**J**) and video 2 (**K**).
505 The merged images at t=0 minutes (cyan) and t=15 minutes (red) highlighted the dramatic
506 increased mobility of microglial cell bodies in the presence of hTau^{P301L}-expressing neurons. (**L-**
507 **N**) Measurements of microglia dynamics; process speed (**L**, $p = 0.0004$), process track
508 displacement (**M**, $p = 0.0002$) and cell body displacement (**N**, $p = 0.0054$), in Tg(ApoE-eGFP)
509 (n=3) and Tg(ApoE-eGFP; HuC-hTau^{P301L}:DsRed) (n=4) embryos, confirmed the increased
510 mobility of both microglia processes and cell bodies observed in the presence of hTau^{P301L}-
511 expressing neurons. (**O, P**) Measurements of pro-inflammatory cytokines in the brain of 5 dpf
512 Tg(ApoE-eGFP) (n=6) and Tg(ApoE-eGFP; HuC-hTau^{P301L}:DsRed) (n=11) embryos. The
513 comparison of relative expressions of IL-1β (**O**, $p = 0.80$) and IL-8 (**P**, $p = 0.89$) in both groups
514 shows no significant differences. (**Q**) Schematic dorsal view of a 7 dpf zebrafish embryo. The
515 red square shows the region of interest that comprises the optic tectum. ***: $p < 0.001$; **: p
516 < 0.01; *= $p < 0.05$. Scale bar (A, B, B', H, I, J, K) = 50 µm, (C, D) = 10 µm. A.U.: arbitrary
517 units.

518

519
520
521
522
523
524
525
526
527

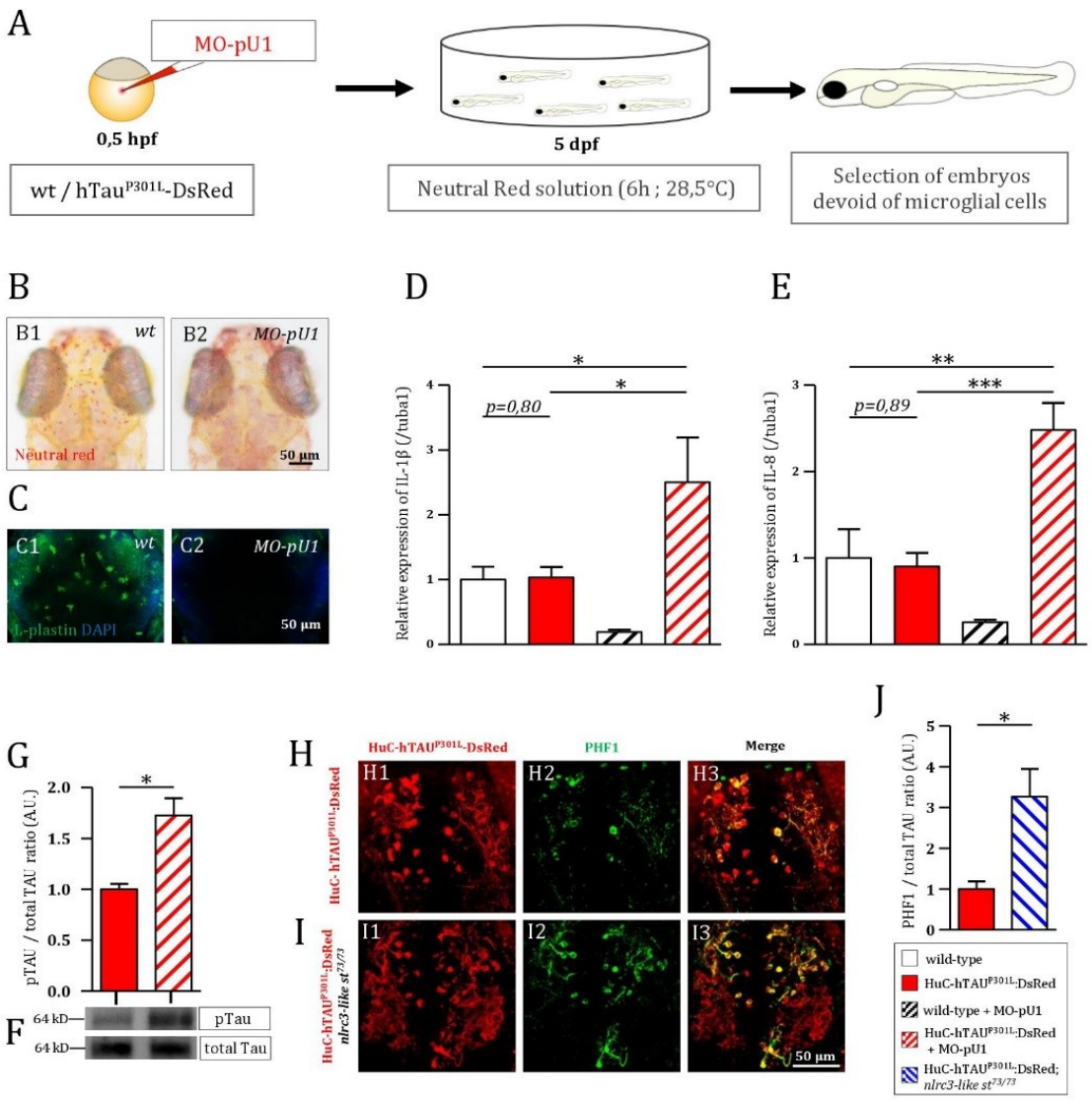

Figure 2. Genetic depletion of microglia worsens the pathology in Tg(HuC-hTau^{P301L}:DsRed) embryos. (**A**) Outline of microglia depletion experiments. Embryos were injected at the single cell stage with a solution of antisense morpholino oligonucleotide targeting pU.1 transcripts. At 5 dpf, injected embryos were incubated in Neutral Red solution to sort microglia-depleted embryos. (**B**) Dorsal views of the optic tectum of 5 dpf wild-type microglia-depleted (**B2**) and untreated live embryos (**B1**), following incubation in Neutral Red solution. (**C**) Dorsal views of the optic tectum of 5 dpf wild-type microglia-depleted (**C2**) and untreated fixed embryos (**C1**), labelled with L-plastin antibody. (**D**, **E**) Measurements of pro-inflammatory cytokines in the brain of 5 dpf wild-type embryos with (n=6), or without (n=3) microglia; and Tg(HuC-hTau^{P301L}:DsRed) embryos with (n=11), or without microglia (n=7). Both relative

555 expressions of IL-1β (**D**, $p = 0.035$) and IL-8 (**E**, $p < 0.0001$) display a significant increase in
556 the brains of Tg(HuC-hTau^{P301L}:DsRed) embryos without microglia cells, compared to Tg(HuC-
557 hTau^{P301L}:DsRed) embryos with microglial cells. (**F**, **G**) Representative Western blots
558 membranes of total protein extracts from 6 dpf Tg(HuC-hTau^{P301L}:DsRed) embryos with (left)
559 or without (right) microglia, hybridated with antibodies against human total Tau (total Tau)
560 or human phosphorylated Tau at Ser396 residues (pTau) (**F**); and quantification of
561 corresponding pTau/total Tau ratio (respectively, n=4 and n=4) (**G**, $p = 0.01$). The ratio of
562 hyperphosphorylated hTau protein is significantly increased in Tg(HuC-hTau^{P301L}:DsRed)
563 embryos that are microglia-depleted with morpholino. (**H-J**) Dorsal views of the telencephalon
564 of 6 dpf Tg(HuC-hTau^{P301L}:DsRed) embryos (**H**) and Tg(HuC-hTau^{P301L}:DsRed; *nlrc3-like*$^{st73/73}$)
565 embryos (**I**), labelled with an antibody against human phosphorylated Tau at Ser396 and Ser404
566 residues (PHF1); and quantification of corresponding PHF1/hTau^{P301L}-DsRed signal ratio
567 (respectively, n=4 and n=6) (**J**, $p = 0.0485$). The quantification of the ratio of
568 hyperphosphorylated hTau protein on brain sections from Tg(HuC-hTau^{P301L}:DsRed; *nlrc3-*
569 *like*$^{st73/73}$) mutant embryos devoid of microglia confirmed the significant increase of this ratio
570 displayed in protein extracts from Tg(HuC-hTau^{P301L}:DsRed) embryos microglia-depleted with
571 morpholino. ***, $p < 0.001$; **, $p < 0.01$; *, $p < 0.05$. Scale bar (B, C, H, I) = 50 µm.

572

573

574

575

576

577

578

579

580

581

582

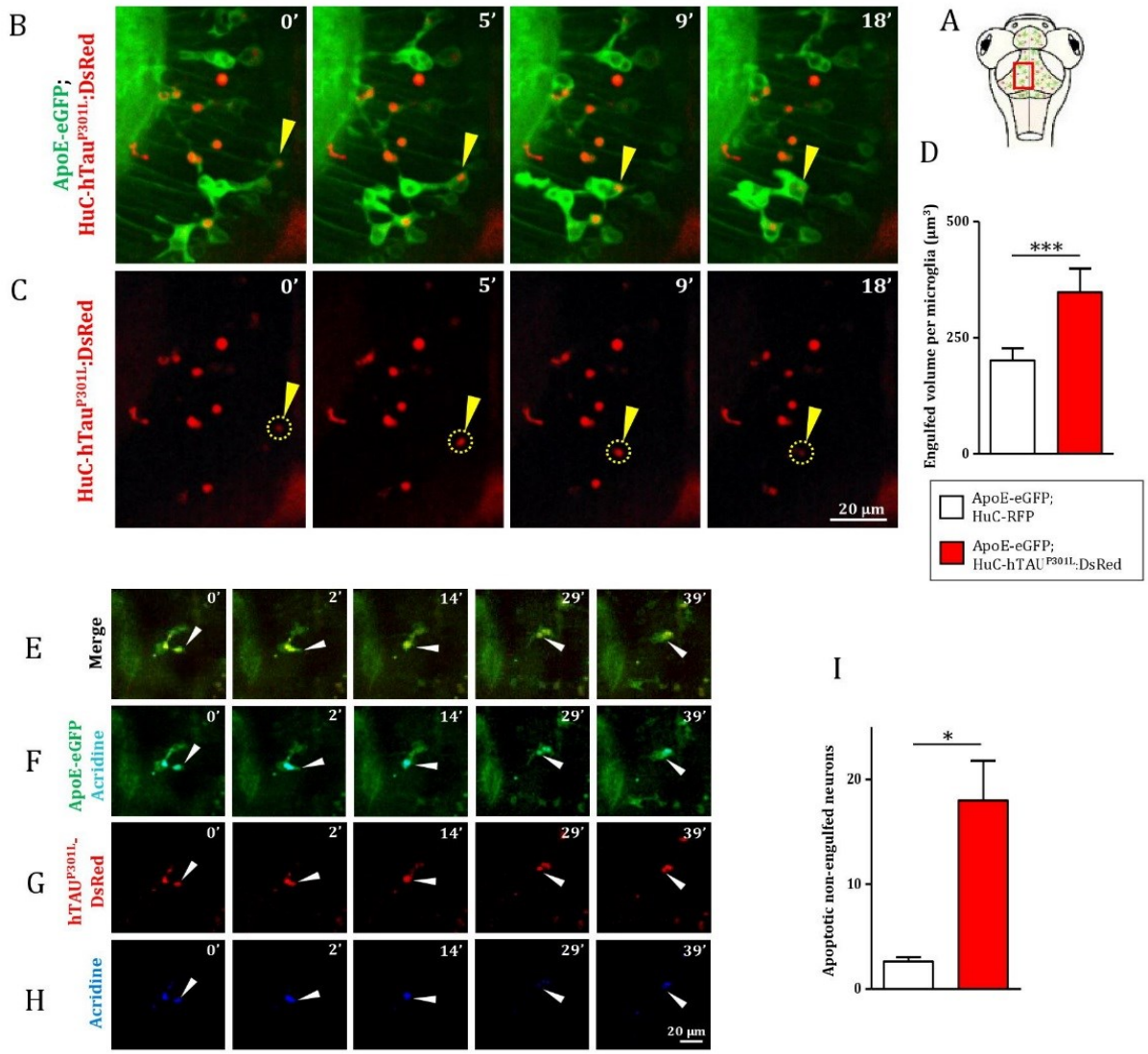

Figure 3. Microglia phagocytic activity is increased in presence of hTau^{P301L}–expressing, but appears non-sufficient in eliminating all apoptotic neurons. (**A**) Schematic illustration of 7 dpf embryo in dorsal view. The red square shows the region of the optic tectum where the time-lapse (**B, C**) was recorded. (**B, C**) Time-lapse imaging of a microglial cell phagocyting a diseased neuron (yellow arrowhead) in a 7 dpf Tg(ApoE-eGFP; HuC-hTau^{P301L}:DsRed) embryo; (**B**, Video 3) merge of GFP and DsRed; (**C**) DsRed only. (**D**, $p = 0.0262$) Quantification of the engulfed neuronal volume in Tg(ApoE-eGFP; HuC-RFP) (n=7) and Tg(ApoE-eGFP; HuC-hTau^{P301L}:DsRed) (n=9) embryos, showing a significantly increased phagocytosis level by microglial cells in the presence of hTau^{P301L}-expressing neurons. (**E-H,** Video 4) Time-lapse image sequences from the optic tectum of a double transgenic Tg(ApoE-eGFP; HuC-hTau^{P301L}:DsRed)

608 7 dpf embryo, showing a detail of a microglial cell in the process of phagocyting a neuron
609 labelled with an apoptosis marker, acridine orange (merge: **E**, GFP and acridine: **F**, DsRed only:
610 **G**, acridine only: **H**). The microglial cell filled with other dead tauopathic neurons extends its
611 process to another dying tauopathic neuron and draws it towards its body cell to complete the
612 phagocytosis process. (**I**, $p = 0.027$), Quantification of the number of non-engulfed apoptotic
613 neurons in Tg(ApoE-eGFP; HuC-RFP) (n=11) and double transgenic Tg(ApoE-eGFP; HuC-
614 hTau^{P301L}:DsRed) (n=4) embryos in which there is a significantly higher number of un-engulfed
615 apoptotic neurons. ***, $p < 0.001$; **, $p < 0.01$; *, $p < 0.05$. Scale bar (B, C, E, F, G, H) = 20
616 µm.

617

618
619
620
621
622
623
624

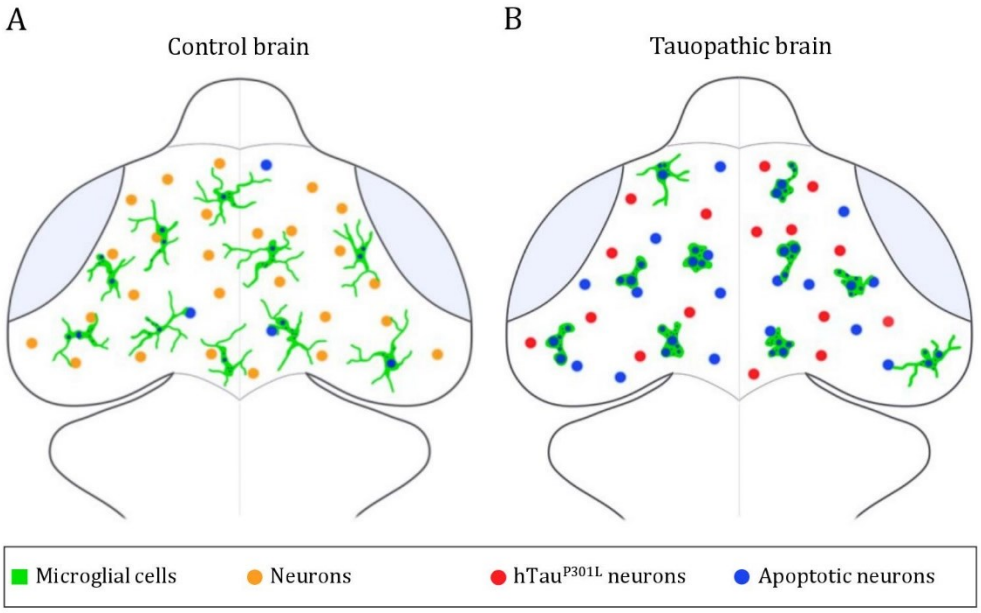

625

626 **Figure 4. Summary illustration.** (**A, B**) Brain illustrations of control embryo (**A**) and
627 tauopathic embryo (**B**). In the control embryo brain, microglial cells (green) display a highly
628 ramified morphology, allowing them to scan the brain and monitor neighbouring neurons
629 (orange) and eliminate apoptotic ones (blue). However, in presence of hTau^{P301L}–expressing
630 neurons (red), microglial cells (green) adopt a noninflammatory amoeboid morphology, that
631 allows them to move faster throughout the brain in order to eliminate tauopathic neurons
632 undergoing apoptosis (blue). In spite of an increased phagocytic rate of microglial cells in the
633 tauopathic brain, there is a higher number of non-engulfed apoptotic neurons (blue), in
634 comparison to the control brain; thus, suggesting a saturated phagocytic capacity of microglial
635 in the tauopathic brain.